Electronic Supplementary Information for

Heterostructured WO_3@$CoWO_4$ bilayer nanosheets for enhanced visible-light photo, electro and photoelectro-chemical oxidation of water

Huayang Zhang [a, 1], Wenjie Tian [a, 1], Yunguo Li [c,1], Hongqi Sun [b, *], Moses O. Tadé [a], and Shaobin Wang [a,*]

[a] Department of Chemical Engineering, Curtin University, GPO Box U1987, Perth, WA 6845, Australia.

[b] School of Engineering, Edith Cowan University, 270 Joondalup Drive, Joondalup, WA 6027, Australia.

[c] Department of Earth Sciences, University College London, Gower Street, London WC1E 6BT, United Kingdom.

* Corresponding Authors.

Email address: shaobin.wang@curtin.edu.au; h.sun@ecu.edu.au

[1] These authors contributed equally to this work.

Materials Characterizations

X-ray diffraction spectra were recorded on an Empyrean multi-purpose research diffractometer (Panalytical Empyrean XRD) using the filtered Cu Kα radiation (λ = 1.5418 Å) with an accelerating voltage of 40 kV and a current of 40 mA. The transmission electron microscopy (TEM) images were obtained on a JEOL 2100 TEM microscope (120 kV) and FEI TITAN G2 (200 kV). The high angle annular dark field scanning transmission electron microscopy (HAADF-STEM) images and EDX mapping analysis were carried out on FEI TITAN G2 (200 kV). X-ray photoelectron spectroscopy (XPS) was conducted under ultrahigh vacuum condition on a Kratos Axis Ultra DLD system. UV-Visible diffuse reflectance spectra and photoluminescence spectra were collected on a Cary 100 UV-Visible Spectrophotometer and a Cary Eclipse Fluorescence Spectrophotometer (Agilent, US) respectively.

Electron paramagnetic resonance (EPR) signals of radicals were trapped by 5, 5-dimethyl-1-pyrroline N-oxide (DMPO) and recorded on a Bruker EMXplus spectrometer. A sample of 40 μL solution containing 0.5 mg/mL catalysts (WO_3 or WO_3@$CoWO_4$-3), 0.05 M Na_2SO_4, 0.01 M $Na_2S_2O_8$ and 0.8 μM $Ru(bpy)_3Cl_2$ was mixed with 40 μL 0.08 M DMPO. After that, the home-made quartz tube with the samples was illuminated under a 100 W Hg lamp. The settings for the EPR spectrometer were as follows: center field (3514.70 G); sweep width (100 G); microwave frequency (9.82 GHz); modulation frequency (200 kHz); power (10.00 mW).

Density Functional Theory (DFT) calculations

Spin-polarized DFT calculations were performed using the Vienna *Ab initio* Simulations Package (VASP) [1, 2] and projected augmented wave (PAW) [3-5] method (with 5*p*, 6*s* and 5*d* treated as valence electrons for W, 3*d* and 4*s* for Co, and 2*s* and 2*p* for O). Generalized gradient approximation (GGA) in the Perdew, Burke and Ernzerhof (PBE) [6] parameterization was used to account for exchange-correlation interaction. The Hubbard U parameters (GGA+U) with U=4.5 eV [7] and 6.0 eV [8] for Co and W, respectively, were used to describe the on-site *d*-electron correlations in $CoWO_4$ (space group *P2/c*, No. 13) and WO_3 (space group *P6/mmm*, No. 191).

For relaxations of bulk WO_3 and $CoWO_4$, the cut-off energy of plane-wave basis was set to 520 eV, and integrations over the first Brillouin zone were made using Gamma-centred k-point sets of 4×4×8 for WO_3 and 4×2×4 for $CoWO_4$. With these settings, the total energy was able to converge within 1 meV/atom. Atomic positions were fully relaxed with the energy converged within 10^{-6} eV/cell and the force converged to less than 10^{-4} eV/Å. Surface calculations used the same cutoff energy and k-point grids as dense as in the bulk calculations (in the case of vacuum direction, only Gamma point was used).

Gibbs free energy changes for the four elementary steps of OER were calculated using following equations: [9, 10]

$$\Delta G_1 = G(*OH) - G(*) - G(OH) = E(*OH) + 0.5E(H_2) - E(*) - E(H_2O) - eU + k_B$$

$$\Delta G_2 = G(*O) + G(H) - G(*OH) = E(*O) + 0.5E(H_2) - E(*OH) - eU + k_B T ln(a_{H+}) + \Delta ZPE - T\Delta S \quad (2)$$

$$\Delta G_3 = G(*OOH) - G(OH) - G(*O) = E(*OOH) - E(*O) + 0.5E(H_2) - E(H_2O) - eU - T\Delta S \quad (3)$$

$$\Delta G_4 = 4 \times \left[1.23\ eV - eU + k_B T ln\left(a_{H+}\right)\right] - \left(\Delta G_1 + \Delta G_2 + \Delta G_3\right) \quad (4)$$

where $E(H_2O)$, $E(*)$, $E(*OH)$, $E(*O)$, and $E(*OOH)$ are DFT total energies on catalytic surfaces without and with *OH, *O and *OOH, respectively. $G(*)$, $G(*O)$, $G(*OH)$, and $G(*OOH)$ are the Gibbs free energies of the surfaces without and with *O, *OH and *OOH groups, respectively. k_B is the Boltzmann constant and T is temperature (300 K). ZPE is the abbreviation of zero-point energy. S denotes entropy. The entropy and ZPE contributions to the Gibbs free energy change are included in the term of $(\Delta ZPE - T\Delta S)$. The used ZPE and entropy values of gaseous and adsorbed OER species are listed in Table S1.

Table S1. Entropy and zero-point energy contributions to Gibbs free energy of gaseous and adsorbed OER species.[11]

Species	ZPE (eV)	TS (eV)
H_2O	0.56	0.67
H_2	0.27	0.41
*OH	0.35	0.0
*O	0.05	0.0
*OOH	0.41	0.0

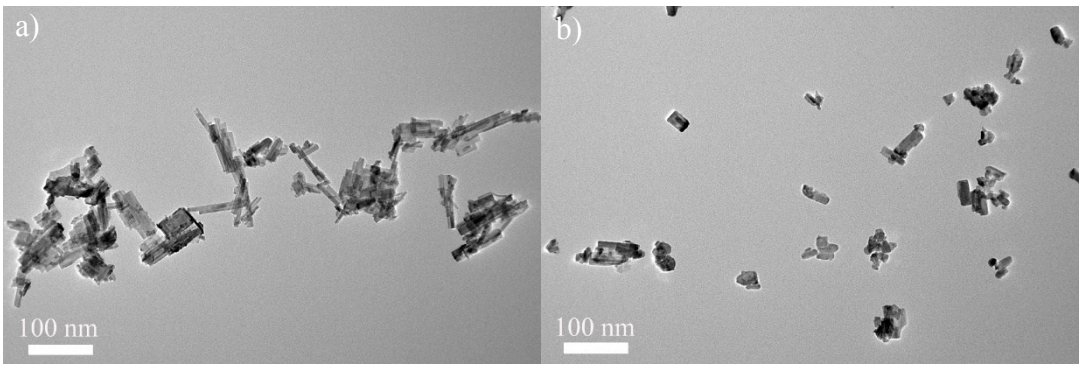

Fig. S1 Low magnitude TEM images of a) WO_3, and b) WO_3@$CoWO_4$-3.

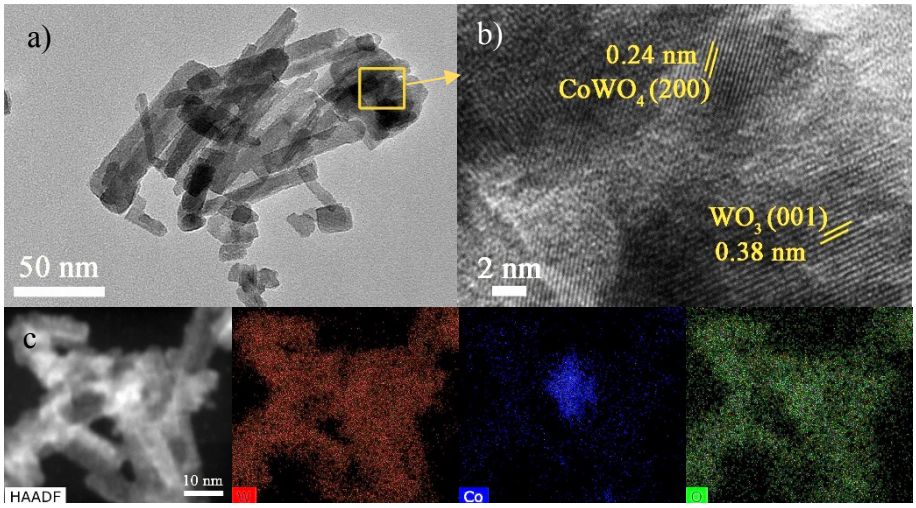

Fig. S2 a) TEM, b) HRTEM, c) HAADF-STEM and the corresponding EDX elemental mapping images of WO_3@$CoWO_4$-1.

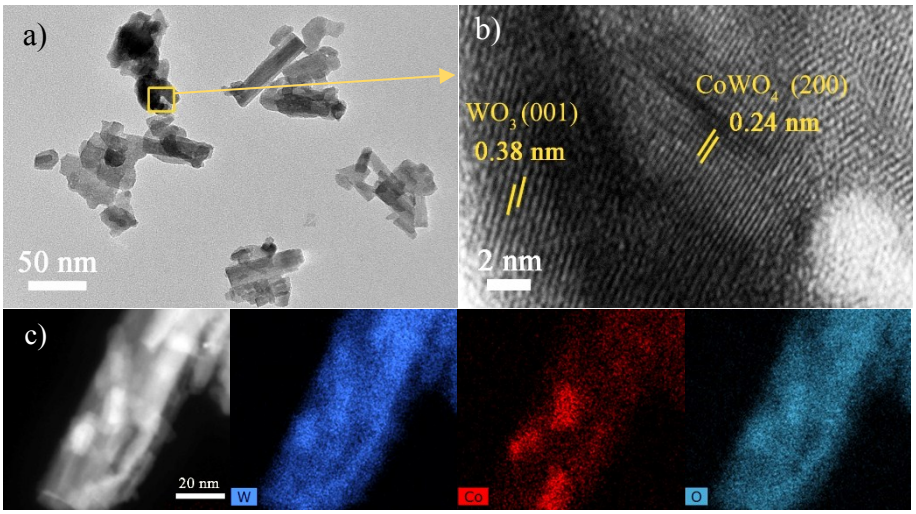

Fig. S3 a) TEM, b) HRTEM, c) HAADF-STEM and the corresponding EDX elemental mapping images of WO_3@$CoWO_4$-2.

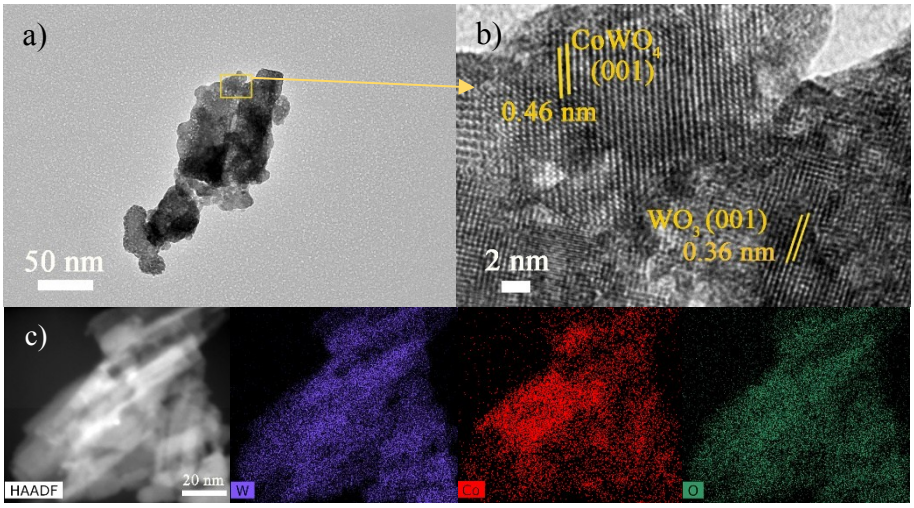

Fig. S4 a) TEM, b) HRTEM, c) HAADF-STEM and the corresponding EDX elemental mapping images of WO_3@$CoWO_4$-4.

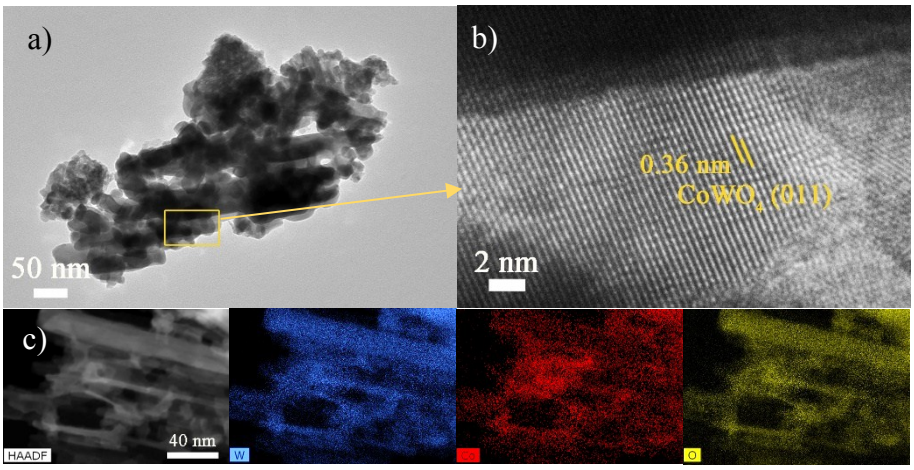

Fig. S5 a) TEM, b) HRTEM, c) HAADF-STEM and the corresponding EDX elemental mapping images of WO_3@$CoWO_4$-5.

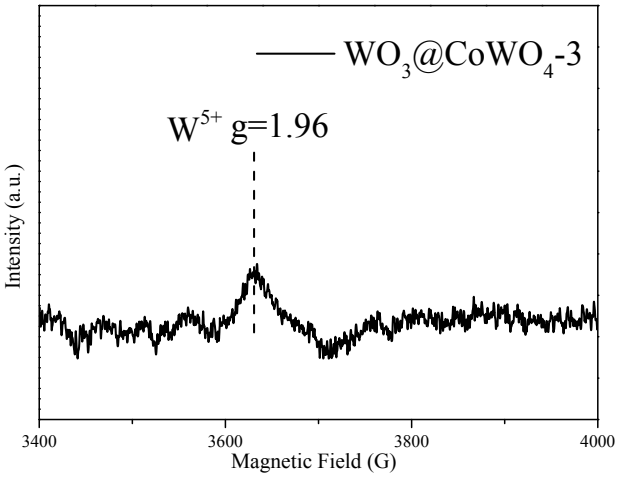

Fig. S6 Solid-state EPR signals of W^{5+} tested on WO_3@$CoWO_4$-3.

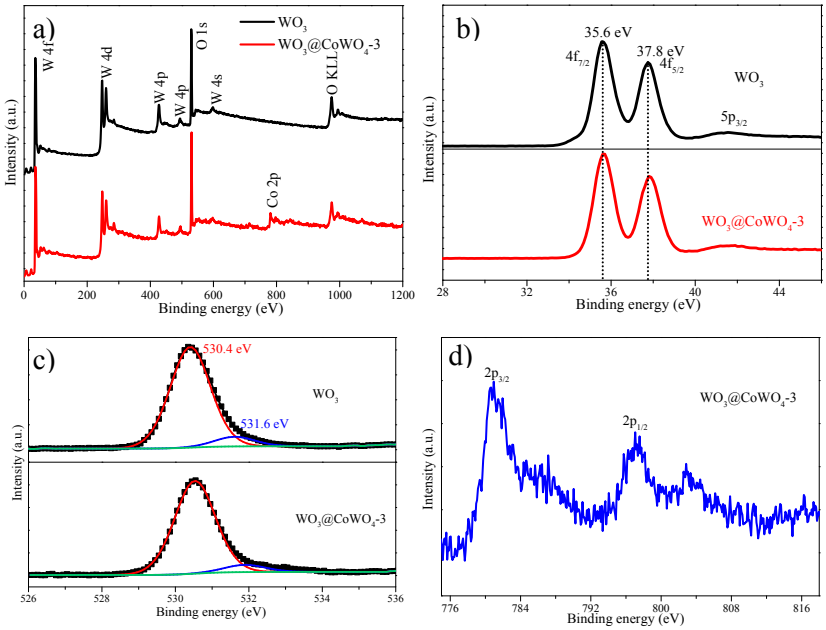

Fig. S7 XPS survey of WO_3 and WO_3@$CoWO_4$-3. a) Full spectra and high-resolution XPS spectra of b) W4f, c) O1s and d) Co2p.

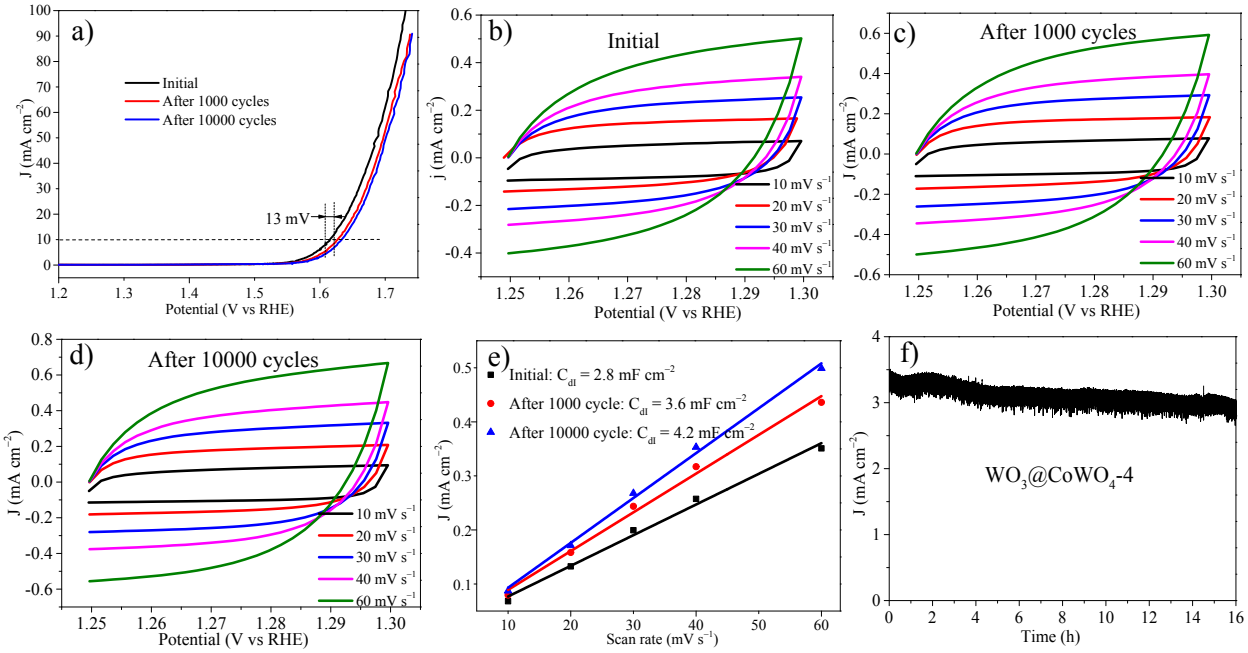

Fig. S8 Durability test on WO_3@$CoWO_4$-4 in 0.1M KOH. a) ADT tests; b-d) CV tests at different scan rates before and after ADT tests of 1000 and 10000 cycles; e) current density as a function of the scan rate before and after ADT tests; f) chronoamperometric response (i-t) of WO_3@$CoWO_4$-4 estimated at 1.614 V (vs. RHE) and 1600 rpm.

As shown in Fig. S8a, after accelerated durability test (ADT) of 1000 cycles, the overpotential of WO_3@$CoWO_4$-4 increased by about 13 mV. Notably, negligible difference was observed after another 9000 cycles, revealing its fairly excellent durability performance. The electrochemical double-layer capacitance (C_{dl}) before and after ADT tests was calculated by measuring CV curves (Fig. S8b-d) to estimate the electrochemical active surface area (EASA). As shown in Fig. S8e, C_{dl} increased from the initial 5.67 to 7.17 and 8.3 mF cm^{-2} after 1000 and 10000 cycles, respectively. The results indicated the stability of the active sites, which is beneficial to catalytic performance. The slight enhancement in ECSA might arise from the changes in the valence states of Co (Co^{2+}/Co^{3+}) and W (W^{5+}/W^{6+}) on the catalyst surface during the ADT tests.[12] The stability of WO_3@$CoWO_4$-4 was also evaluated by measuring Chronoamperometric response (i-t), which showed a little decay (17%) of J over 16 h (Fig. S8f).

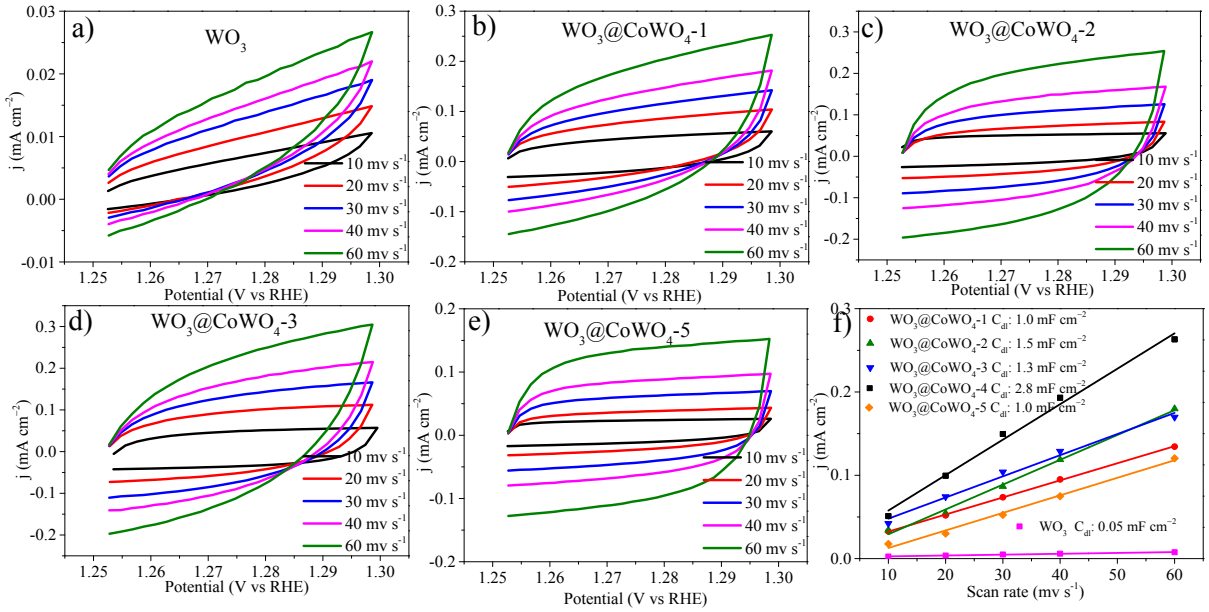

Fig. S9 a-e) CV tests at different scan rates and f) current density as a function of scan rate.

Table S2 Photocatalytic activities of metallic OER catalysts for O_2 evolution.

Catalyst	Catalyst addition amount (mg)	Irradiation wavelength (nm)	Oxygen evolution (mmol/g)	Irradiation time (h)	Reference
WO_3–RGO	50	>420 nm	0.23	5	[13]
0.001 wt% RuO_2/WO_3	100	>420 nm	1.4	4	[14]
3 wt% $Co(OH)_2$-TiO_2	100	＞500nm	0.4	10	[15]
$PtOx/WO_3$	100	>350 nm	0.279	3	[16]
$Pt(0.5)/Au(3.0)/WO_3$	50	Blue LED	0.036	1	[17]
Bulk WO_3	50	>400 nm	0.796	1	[18]
WO_{3-X}-HT	100	>400 nm	0.75	1	[19]
RuO_2/Bi_4TaO_8X (X = Cl, Br)	100	>420 nm	0.375	1	[20]
(0.1%) RuO_2/α-Fe_2O_3/2D g-C_3N_4/Pt (3%)	50	>400 nm	0.19	5	[21]
CoS	50	>420 nm	1.866	0.2	[22]
MoO_2 -HTCC	30	>420 nm	0.7	25	[23]
mWO_3/AuNP	2.5	>400 nm	0.065	0.067	[24]
WO_3@$CoWO_4$–3	**50**	**>420 nm**	**1.6**	**1**	**This work**

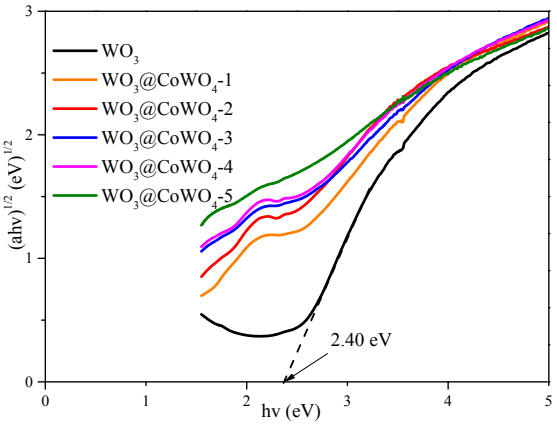

Fig. S10 Tauc's plots of the samples acquired from the adsorption spectra (Fig. 5b) based on Kubelka-Munk equation: (αhν)n = k(hν-Eg) (n=1/2).

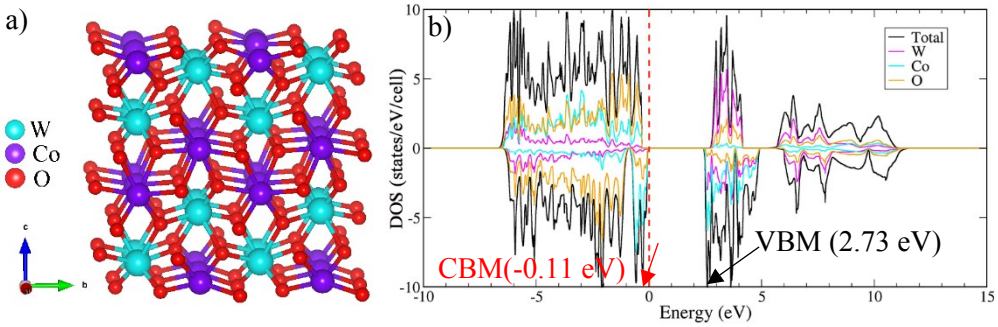

Fig. S11 a) Atomic models of monoclinic $CoWO_4$ (M-1) and b) its corresponding density of states (DOS).

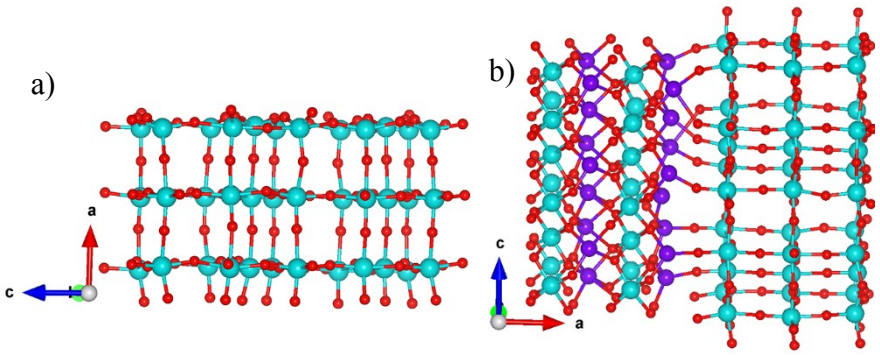

Fig. S12 Molecular models of a) hexagonal WO_3 slab (M-2) and b) WO_3@$CoWO_4$ slab (M-3).

Construction of M-3

The (200) planes of $CoWO_4$ and the (001) planes of WO_3 were selected to construct the interface in M-3, as TEM images (Fig. 2d, S2b and S3b) have revealed the close atomic bonding between the two planes and they possess a small planar mismatch (~0.8%) while there is a remarkable lattice mismatch in other combinations. The general oxidation states of Co and W in $CoWO_4$ are +2 and +6, respectively,

suggesting that the bonding between W and O is much stronger than that between Co and O.[7] In this regard, it requires more energy to break up the W-O bond than the cleavage of Co-O bond. Therefore, compared with W (200) surface, Co (200) surface of $CoWO_4$ is more likely to bond with WO_3. The stoichiometric WO_3@$CoWO_4$ heterogeneous structure was built in Fig. S12b with Co-terminated (200) surface of $CoWO_4$ connected with O-terminated (001) surface of WO_3, containing 228 atoms. The M-3 has a composition close to WO_3@$CoWO_4$-3.

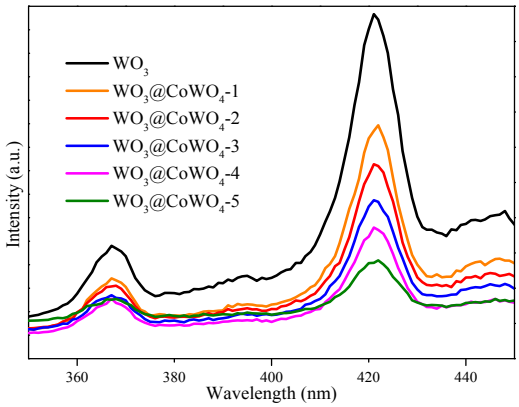

Fig. S13 Photoluminescence (PL) spectra of pure WO_3 and the composites.

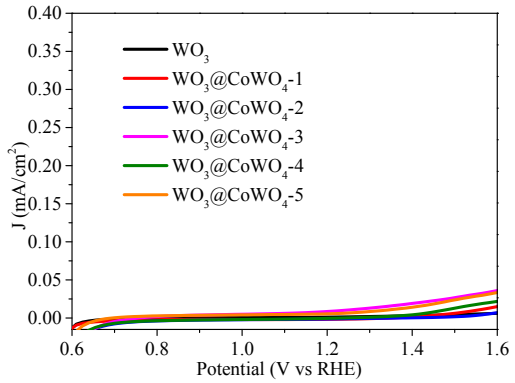

Fig. S14 Current-voltage curves of the composites in the dark.

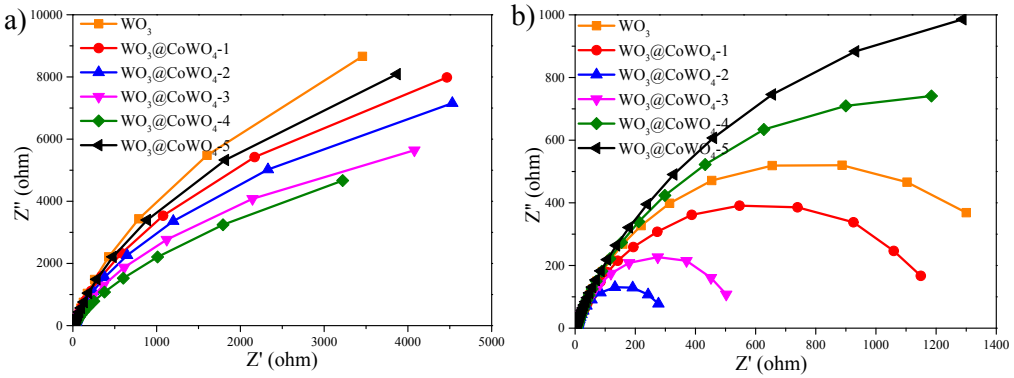

Fig. S15 Electrochemical impedance spectra collected under a) dark and b) irradiation condition.

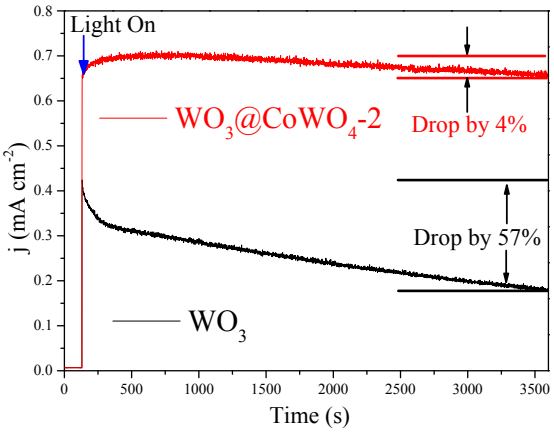

Fig. S16 Potentiostatic measurement of WO_3 and WO_3@$CoWO_4$-2 at 1.23 V (vs RHE) under irradiation for 1 h.

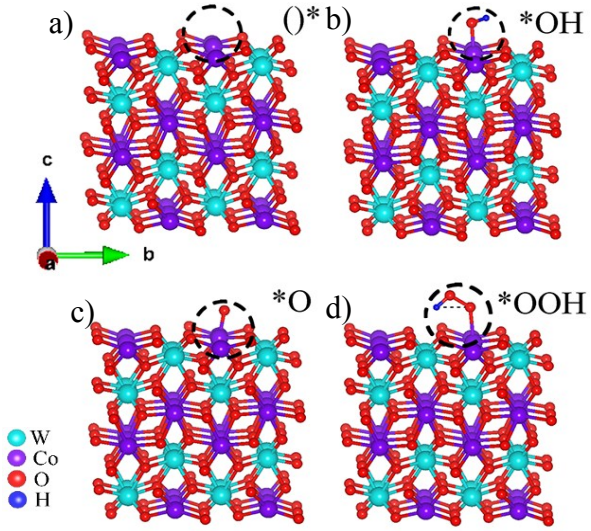

Fig. S17 $CoWO_4$ slab (M-1) with the adsorbed species generated in OER.

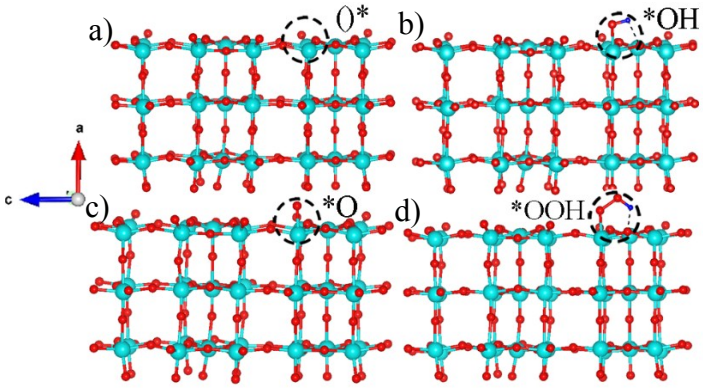

Fig. S18 WO_3 slab (M-2) with the adsorbed species generated in OER.

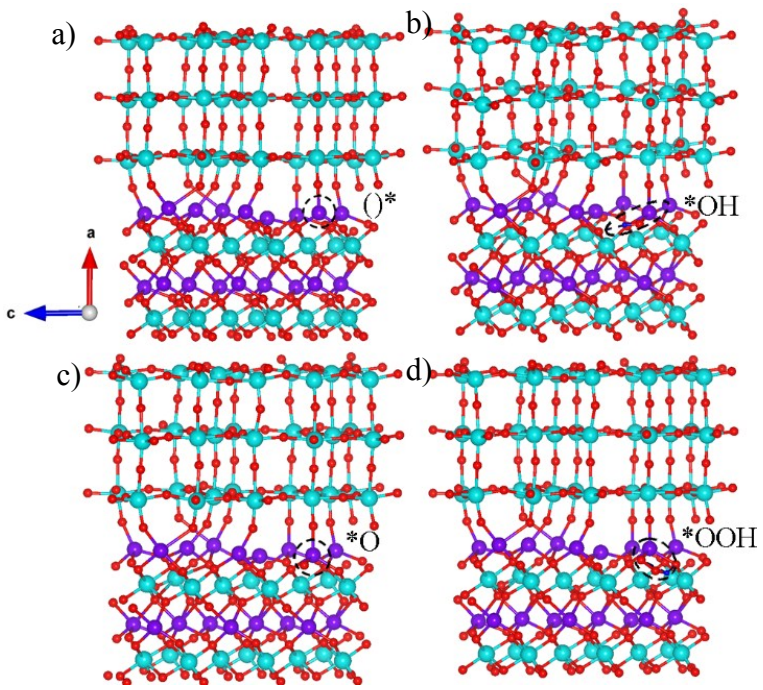

Fig. S19 WO_3@$CoWO_4$ slab (M-3) with the adsorbed species generated in OER.

Table S3 Gibbs free energy changes during the four elementary steps of OER (U = 0 and pH= 7).

Model	ΔG_1	ΔG_2	ΔG_3	ΔG_4
M-1	2.02	2.00	0.11	-0.82
M-2	1.27	1.51	0.80	-0.27
M-3	1.23	1.42	0.77	-0.11
M-4	0.47	0.83	1.51	0.48

References

1 G. Kresse and D. Joubert, *Phys. Rev. B*, 1999, **59**, 1758−1775..
2 P. E. Blöchl, *Phys. Rev. B*, 1994, **50**, 17953−17979.
3 G. Kresse and J. Furthmüller, *Comput. Mater. Sci.*, 1996, **6**, 15−50.
4 G. Kresse and J. Furthmüller, *Phys. Rev. B*, 1996, **54**, 11169−11186.
5 G. Kresse and J. Hafner, *Phys. Rev. B*, 1993, **48**, 13115−13118.
6 J. P. Perdew, K. Burke and M. Ernzerhof, *Phys. Rev. Lett.*, 1996, **77**, 3865−3868.
7 C. Ling, L. Q. Zhou and H. Jia, *RSC Adv.*, 2014, **4**, 24692−24697.
8 N. Bondarenko, O. Eriksson and N. V. Skorodumova, *Phys. Rev. B*, 2015, **92**, 165119.
9 I. C. Man, H.-Y. Su, F. Calle-Vallejo, H. A. Hansen, J. I. Martínez, N. G. Inoglu, J. Kitchin, T. F. Jaramillo, J. K. Nørskov and J. Rossmeisl, *ChemCatChem*, 2011, **3**, 1159−1165.
10 Y. Li, Y.-L. Li, B. Sa and R. Ahuja, *Catal. Sci. Tech.*, 2017, **7**, 545−559.
11 Á. Valdés, Z. W. Qu, G. J. Kroes, J. Rossmeisl and J. K. Nørskov, *J. Phys. Chem. C*, 2008, **112**, 9872−9879.
12 Y. L. Zhu, W. Zhou, J. Sunarso, Y. J. Zhong and Z. P. Shao, *Adv. Funct. Mater.*, 2016, **26**, 5862−5872.

13 H. Huang, Z. Yue, G. Li, X. Wang, J. Huang, Y. Du and P. Yang, *J. Mater. Chem. A*, 2013, **1**, 15110−15116.
14 S. S. K. Ma, K. Maeda, R. Abe and K. Domen, *Energy Environ. Sci.*, 2012, **5**, 8390−8397.
15 K. Maeda, K. Ishimaki, Y. Tokunaga, D. Lu and M. Eguchi, *Angew. Chem. Int. Ed. Engl.*, 2016, **128**, 8449−8453.
16 K. Maeda, D. Lu and K. Domen, *ACS Catal.*, 2013, **3**, 1026−1033.
17 A. Tanaka, K. Hashimoto and H. Kominami, *J. Am. Chem. Soc.*, 2014, **136**, 586−589.
18 M. R. Waller, T. K. Townsend, J. Zhao, E. M. Sabio, R. L. Chamousis, N. D. Browning and F. E. Osterloh, *Chem. Mater.*, 2012, **24**, 698−704.
19 J. Yan, T. Wang, G. Wu, W. Dai, N. Guan, L. Li and J. Gong, *Adv. Mater*, 2015, **27**, 1580−1586.
20 X. Tao, Y. Zhao, L. Mu, S. Wang, R. Li and C. Li, *Adv. Energy Mater.*, 2017, **8**, 1701392.
21 X. She, J. Wu, H. Xu, J. Zhong, Y. Wang, Y. Song, K. Nie, Y. Liu, Y. Yang, M.-T. F. Rodrigues, R. Vajtai, J. Lou, D. Du, H. Li and P. M. Ajayan, *Adv. Energy Mater.*, 2017, **7**, 1700025.
22 M. Zheng, Y. Ding, L. Yu, X. Du and Y. Zhao, *Adv. Funct. Mater.*, 2017, **27**, 1605846.
23 Z. Hu, G. Liu, X. Chen, Z. Shen and J. C. Yu, *Adv. Funct. Mater.*, 2016, **26**, 4445−4455.
24 B. Liu, C. H. Kuo, J. Chen, Z. Luo, S. Thanneeru, W. Li, W. Song, S. Biswas, S. L. Suib and J. He, *Angew. Chem. Int. Ed. Engl.*, 2015, **54**, 9061−9065.